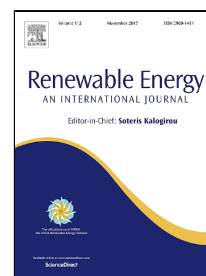


# Accepted Manuscript

Theoretical and numerical study on performance of the air-source heat pump system in Tibet

Yongcai Li, Wuyan Li, Zongsheng Liu, Jun Lu, Liyue Zeng, Lulu Yang, Ling Xie



PII: S0960-1481(17)30649-3

DOI: 10.1016/j.renene.2017.07.036

Reference: RENE 9011

To appear in: *Renewable Energy*

Received Date: 24 November 2016

Revised Date: 06 July 2017

Accepted Date: 10 July 2017

Please cite this article as: Yongcai Li, Wuyan Li, Zongsheng Liu, Jun Lu, Liyue Zeng, Lulu Yang, Ling Xie, Theoretical and numerical study on performance of the air-source heat pump system in Tibet, *Renewable Energy* (2017), doi: 10.1016/j.renene.2017.07.036

This is a PDF file of an unedited manuscript that has been accepted for publication. As a service to our customers we are providing this early version of the manuscript. The manuscript will undergo copyediting, typesetting, and review of the resulting proof before it is published in its final form. Please note that during the production process errors may be discovered which could affect the content, and all legal disclaimers that apply to the journal pertain.

# Theoretical and numerical study on performance of the air-source heat pump system in Tibet

Yongcai Li, Wuyan Li, Zongsheng Liu, Jun Lu,\* Liyue Zeng, Lulu Yang, Ling Xie

Key Laboratory of the Three Gorges Reservoir Region's Eco-Environment, Ministry of Education,  
Chongqing University, Chongqing, 400045, China

\*Corresponding author: Prof. Jun Lu

Contact address: Faculty of the Urban Construction & Environment Engineering, Chongqing  
University, 400030, China

Email: [905255911@163.com](mailto:905255911@163.com), Tel: +86(0)23 6512 3777

## ABSTRACT

Air source heat pump (ASHP) technology is widely accepted for the merits of energy-saving and environmental protection, and has been served as the heating and cooling source in most part of China. This paper presents a numerical model to predict the performance of a typical ASHP system in Lhasa, the capital of Tibet Autonomous Region of China. The theoretical analysis shows that the occurrence of the frost is hard to be found on air-side heat exchanger due to the low relative humidity, which can improve the performance of the ASHP system. The numerical results show that the ambient air temperature and atmospheric pressure have a great effect on the system performance. For the case of without considering frosting problem, the COP of the system is reduced by 9.5 % - 12.5 % than that for standard pressure (101.325

23 kPa). The heating capacity of the system is reduced by 16.2 % to 19.8 % than that for  
 24 standard pressure. For the case of considering frosting problem, the heating capacity  
 25 and COP of the ASHP system in Lhasa are 37.5 kW and 1.98, respectively under the  
 26 outdoor design temperature, which are almost same or higher than most cities in this  
 27 study.

28 Keywords: Air source heat pump; atmospheric pressure; ambient temperature;  
 29 frosting problem; COP; heating capacity

# Nomenclature

$A_c$	the area of the condenser ( $m^2$ )	$p_s$	the partial pressure of saturated water vapor (Pa)
$C_p$	the specific heat at constant pressure ( $J/kg \cdot K$ )	$p_{tp}$	the pressure of triple-phase point (Pa)
$C_v$	the specific heat at constant volume ( $J/kg \cdot K$ )	$p_v$	the partial pressure of water vapor (Pa)
$C_{val}$	the characteristic constant of the expansion valve	$Q_{fe}$	the heat absorption of the finned-tube evaporator (J)
$C_w$	the specific heat of water ( $J/kg \cdot K$ )	$R$	the gas constant ( $J/kg \cdot K$ )
$d_i$	the inner diameter of the tube (m)	$Re$	Reynolds Number
$f$	the friction coefficient	$T$	air temperature (K)
$h$	the enthalpy of gas (J)	$T_a$	the ambient temperature of air ( °C)
$h_a$	the air-side heat transfer coefficient ( $W/m^2 \cdot K$ )	$T_d$	the dew-point temperature ( °C)
$h_c$	the single-phase heat transfer coefficient ( $W/m^2 \cdot K$ )	$T_f$	the sublimation point for the water vapor in air under pressure of $p_v$ (K)
$h_r$	the two-phase heat transfer coefficient of refrigerant inside the evaporator ( $W/m^2 \cdot K$ )	$T_{tp}$	the temperature of triple-phase point ( °C)
$h_w$	the water side heat transfer coefficient ( $W/m^2 \cdot K$ )	$T_w$	the temperature of surface ( °C)
$l$	the mean free path of the gas molecules (m)	$u$	molecular energy (J)
$m_w$	the mass of water (kg/s)	$\bar{u}$	the average velocity of the gas molecules(m/s)
$m_r$	the mass flow rate of refrigerant (kg/s)	$U_c$	the total heat transfer coefficient of condenser ( $W/m^2 \cdot K$ )
$n$	the compressor speed	$U_{fe}$	the total heat transfer coefficient of the evaporator ( $W/m^2 \cdot K$ )

$Nu$	Nuselt number	$\nu$	specific volume ( $\text{m}^3/\text{kg}$ )
$p$	air pressure (Pa)	$V_d$	the displacement volume of compressor ( $\text{cm}^3$ )
$p_b$	the pressure of thermal bulb (Pa)		
$Pr$	Prandtl number	$W_{in}$	electrical input power (KW)
Greek letters			
$\Delta P$	the pressure difference between the inlet and outlet of the expansion valve (Pa)	$\lambda_r$	thermal conductivity ( $\text{W}/\text{m}\cdot\text{K}$ )
$\Delta P_{st}$	the static pressure provided by the valve's spring (Pa)	$\mu$	Dynamic viscosity ( $\text{N}\cdot\text{s}/\text{m}^2$ )
$\Delta T_m$	the log-mean temperature difference ( $^{\circ}\text{C}$ )	$\rho$	density ( $\text{kg}/\text{m}^3$ )
$\eta_{is}$	the isentropic efficiency	$\nu$	Kinematic viscosity ( $\text{m}^2/\text{s}$ )
$\eta_v$	the volumetric efficiency	$\varphi$	the relative humidity of air
Subscripts			
$a$	ambient air	$in$	input
$c$	condenser	$is$	isentropic
$com$	compressor	$s$	saturated water vapor
$con$	condenser	$tp$	triple-phase point
$d$	dew point	$v$	water vapor/
$e$	evaporator	$val$	the expansion valve
$f$	refrigerant liquid/ sublimation point	$w$	air-side heat exchanger surface/water
$i$	ice	$1-4$	state points of refrigerant

30

## 31 1. Introduction

32 Tibet has an average altitude of more than 4000 m above sea level, and is  
33 therefore called the “Roof of the World” and the “Third Pole of the Earth” [1]. Tibet  
34 is characterized by the complex and varied topographic and geological features,  
35 fragile ecology and adverse weather condition [2]. Though Chinese government has  
36 adopted strict policies to protect the unique ecosystem of Tibet, rapid economic  
37 growth and the development of people's living standard, which inevitably brings  
38 increase in energy demand and pollution, are putting pressure on it. Thus, the issue of

increasing energy consumption in Tibet Plateau has aroused more and more interests of researchers and policy makers [3–7]. Tibet lacks the conventional fossil fuel energy resources, most of the coal, oil and gas are transported by road or pipeline from at least 1000 km away. Energy consumption in Tibet is dominated by traditional biomass, such as cattle dung, firewood and crop straw. Most biomass is directly burned as fuel for cooking and heating. The rarefied Tibetan atmosphere and use of outdated stoves, result in a very low burning efficiency, utilizing less than 10% of the potential energy of biomass [8]. Biotic energy sources are becoming overused with the rapid urbanization, and excessive depletion of biotic energy sources is the main factor responsible for deforestation, land desertification, soil erosion, grassland degradation and soil fertility reduction in Tibet [4, 9]. Thus, searching for a green-on-site, efficient device to improve building indoor environment and living conditions is important for Tibet.

Traditionally, boilers are the most commonly used device to meet the heat demand in cold regions in China, which have low energy efficiency and lead to serious air pollution [10–12]. Compared to boilers, Air source heat pump (ASHP) technology is widely accepted for the merits of energy-saving and environmental protection [13]. As a renewable energy, high efficient, structurally simple device as well as having low initial installation cost [14], ASHP would be a promising alternative of heating technology in Tibet.

Experimental and numerical studies on ASHP have been carried out in terms of

the climate conditions around world. Ibrahim et al. [15] presented a dynamic model to assess the performance of an ASHPWH (air source heat pump water heater) in the Lebanese context. The obtained results showed that for the four Lebanese climatic zones, the expected monthly values of the average COP (coefficient of performance) varies from 2.9 to 5, leading to high efficiencies compared with conventional electric water heaters. A numerical study was reported on the integration of photovoltaic/thermal collector (PV/T) with ASHP in Canada. The results showed the system has a potential to annually saving \$500 in electricity bills and 225 kg net reduction in carbon dioxide [16]. The long-term performance testing on air-to-air ASHP was performed at the Technical University of Nova Scotia in Halifax, Canada [17]. It was observed that the COP of the system was 1.8 and 1.1 corresponding to outdoor air temperature 4.5 °C and -15 °C, respectively. Wu et al. [18] carried out a year-round simulation and techno-economic analysis to assess the energy saving potential of an air source absorption heat pump (ASAHP) combining a conventional boiler in different cities in China. Results showed that the energy saving rate (ESR) can reach 21.6% in Harbin, 24.3% in Shenyang, 26.2% in Beijing and 26.3% in Zhengzhou and ESR did not decrease much when the relative design capacity of ASAHP is within 50–100%.

However, the previous work on the topic only focused on the performance of the ASHP is usually based on atmospheric conditions at sea level. The available performance data of ASHP from manufacturers is hence not recommended directly

applying in a situation like Tibet. To the author's knowledge, no public research on the performance of ASHP at significantly high altitudes was found. Therefore, the influence of the climatic parameters on the ASHP performance in such high altitude area needs to be investigated by devised methods before its wide applications.

In this paper, a theoretical and numerical study is performed to assess the ASHP performance in the Tibetan climate, which is a subject with practical relevance when operating ASHP system at significantly high altitudes. The mechanism of frosting formation on evaporator is carried out by theoretical research. Then, a parametric study is carried out to illustrate how the atmospheric pressure and ambient air temperature affect the ASHP performance by using the developed model. Finally, the application feasibility of ASHP in Tibet is analyzed by comparing the COP and heating capacity with those in other cities at low altitude in China.

## **2. Theoretical analysis**

### **2.1. Effect of low air pressure on the physical properties of air**

The physical properties of air closely related to the subject of this study are density, dynamic viscosity, kinematic viscosity, thermal conductivity, specific heat and Prandtl number. How the atmospheric pressure affects these parameters is theoretically explained as below.

*Air density,  $\rho$*

The atmospheric pressure has a direct and fundamental impact on the air density. Assuming the air is ideal gas, the relationship between air density and atmospheric pressure is expressed as bellow [19].

$$\rho = \frac{1000p}{RT} \left(1 - 0.378 \frac{p_v}{p}\right) \quad (1)$$

where  $T$  represents the air temperature at different altitudes,  $R$  is the gas constant, the value of 287.05 is theoretically determined,  $p$  is the air pressure at different altitudes,  $p_v$  is the partial pressure of water vapor.

The relationship between atmospheric pressure and altitudes can be expressed as [20]:

$$p = p_0 \times \left(1 - \frac{0.0065h}{288.15}\right)^{5.25588} \quad (2)$$

where  $p_0$  is standard atmospheric pressure, 101.325 kPa,  $h$  is the altitude.

The calculating equations for the partial pressure of water vapor  $p_v$  are expressed as [19]:

$$p_v = \begin{cases} p_{v,w} \\ P_{v,i} \\ [(40.0 + T_d) \times p_{v,w} - \end{cases} \quad (3)$$

In the above equation,  $p_{v,w}$  is saturated water vapor pressure,  $p_{v,i}$  is the saturated



vapor pressure of ice,  $T_d$  is the dew-point temperature.

Taking Equation (2), Equation (3) into Equation (1), and the variation trends of air density with the altitude is given in Fig.1.

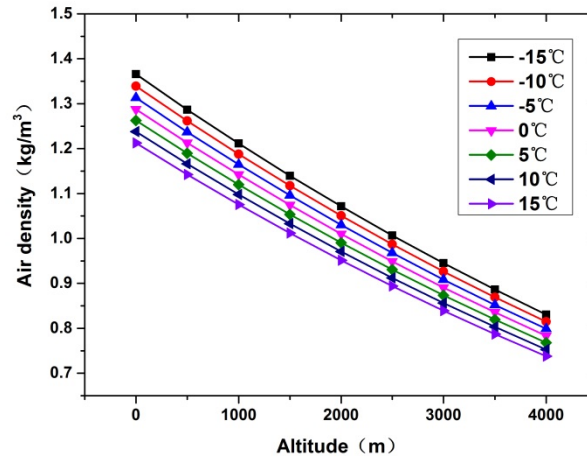


**Fig.1.** The relationship between air density and altitude

It is seen in Fig.1 that the air density is proportional to the atmospheric pressure under certain temperatures, and it is also shown that the air density is decreased with the ambient air temperature increases.

*Specific heat,  $C$*

As the molecular energy and the enthalpy for ideal gas are only related to the temperature, the specific heat of air can be regarded as a single valued function of the temperature in the general pressure variation range (0~1atm), and can be used as a fixed value when the gas temperature is constant and not too high [21].

*Thermal conductivity,  $\lambda$*

Thermal conductivity is the property of a material to conduct heat.

According to the theory of fluid molecules, the thermal conductivity of the air can be considered as constant in certain pressure ranges ( $2.67 \times 10^{-3} \text{MPa} < P < 2 \times 10^3 \text{MPa}$ ) when the temperature is unchanged [22].

*Kinematic viscosity,  $\nu$*

The kinematic viscosity is the ratio of the dynamic viscosity,  $\mu$  to the density of the fluid,  $\rho$ .

$$\nu = \frac{\mu}{\rho}$$

(4)

According to the theory of fluid molecules, the dynamic viscosity of the fluid can be considered to be independent of the pressure at certain temperature [22]. According to the definition of kinematic viscosity, kinematic viscosity is inversely proportional to the density when the dynamic viscosity is unchanged, meaning that it increases with the decrease of the atmospheric pressure. It can be calculated from Eq. (1) and Eq. (4).

*Prandtl number,  $Pr$*

The Prandtl number,  $Pr$ , a dimensionless number, is defined as the ratio of kinematic viscosity ( $\nu$ ) to thermal diffusivity ( $\alpha$ ). That is, the Prandtl number is given as:

$$Pr = \frac{\nu}{\alpha} = \frac{C_p \mu}{\lambda} \quad (5)$$

As previously analyzed,  $C_p$ ,  $\lambda$  and  $\mu$  can be regarded as fixed values when altitude changing, so the Prandtl number is not affected by the altitude.

In summary, the atmospheric pressure affects the air density and kinematic viscosity among the physical properties of air, other physical parameters can be regarded as constant in the following numerical study.

## 2.2. Evaporator frosting characteristics

When a heat pump operates under heating mode in winter, the frost will form on the surface of the outdoor heat exchanger as heat exchanger surface temperature is lower than the outdoor air dew point temperature. The frosting characteristics are one of most important factors which influence the heating performance of ASHP in winter, as frost layer will increase thermal resistance between air and the evaporator. Therefore, the heat exchange rate of the evaporator will decrease and in turn lead to the reduction of the system heating capacity and COP. In this section, the mechanism of frosting formation is theoretically studied under climatic conditions of the representative city, Lhasa, capital of Tibet Autonomous Region of China, where the average altitude is 3680 m.

In order to analyze the mechanism of the frosting, the following assumptions are made:

- (1) The air cleanliness and the wettability of the outdoor heat exchanger surface are not considered because they are difficult to quantify;

(2) The mass flow rate of the refrigerant is evenly distributed to each refrigerant circuit;

(3) A constant speed compressor is used in this study.

As shown in Fig.2, the water can be divided into three single-phase regions (i.e., solid, liquid and gas) with three two-phase boundaries (i.e., solid-liquid, liquid-gas, and solid-gas). The crossover point of three phase boundaries is called triple-phase coexistence point. The temperature of triple-phase point,  $T_{tp}$  in Lhasa is 273.16 K, while the corresponding atmospheric pressure is 611.2 Pa.

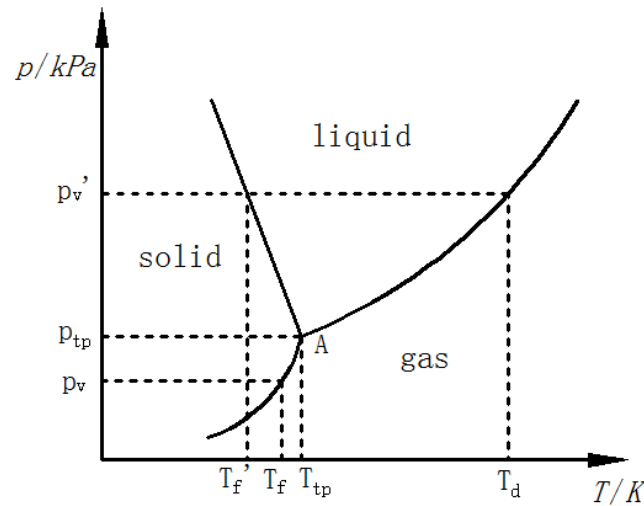


**Fig.2.** The phase diagram of water

When the partial pressure of water vapor,  $p_v < \text{triple-phase point}, p_{tp}$ ,  $T_f$  is the sublimation point for the water vapor in air under pressure of  $p_v$ . If the air-side heat exchanger surface temperature  $T_w > T_f$ , meaning that the condensing or frosting would not occur on the heat exchanger surface. While  $T_w < T_f$ , the water vapor will be directly frosting on heat exchange surface.

When the partial pressure of water vapor  $p_v' > p_{tp}$ ,  $T_f'$  is the freezing (melting) point for the water vapor under pressure of  $p_v'$ . Similarly, if the air-side heat exchanger surface temperature,  $T_w > T_d$ , meaning that the condensing phenomenon would not occur. If  $T_f' < T_w < T_d$ , the condensing will be found, while  $T_w < T_f'$ , the frosting phenomenon will occur.

Based on the analysis above, the frosting characteristics of an ASHP system operating in winter is investigated by using a set of typical daily weather data of January 6 for Lhasa, which is characterized by low outdoor air temperature and high relative humidity [23].

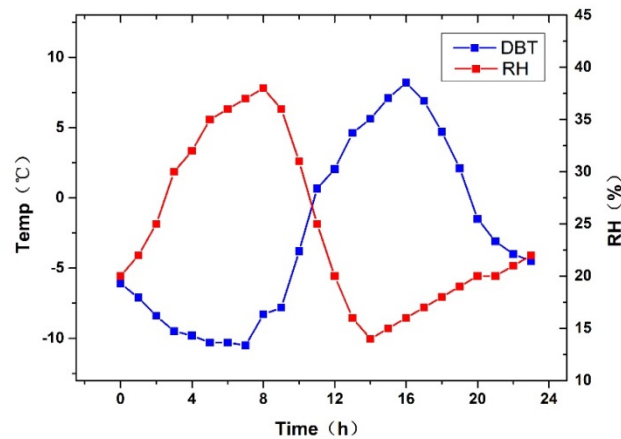


**Fig.3.** The dry bulb temperature and relative humidity of typical daily weather data in Lhasa

As shown in Fig.3, the air dry bulb temperature reaches its minimum value of -10.3°C at 7:00am, and then it rises to the maximum value of 8.2°C at 16:00 pm. However, the variation trend of the relative humidity is contrary to that of the dry bulb temperature. The relative humidity rises to the maximum value of 38% at 8:00am, and

then it reduces to the minimum value of 15% at 15:00 pm.

According to the Eq. (2), the atmospheric pressure for Lhasa is 64.3 KPa, which accounts for only 63% of that for sea level. The partial pressure of water vapor,  $P_v$ , can be calculated by using the following equation:

$$P_v = \varphi \cdot P_s \quad (6)$$

Where  $\varphi$  is the relative humidity of air,  $P_s$  is the partial pressure of saturated water vapor, Pa.

Fig.4 depicts the variation profiles of the partial pressure of water vapor, partial pressure of saturated water vapor and triple point' corresponding pressure. It is seen that the partial pressure of saturated water vapor varies between 310 to 1085Pa, and the partial pressure of water vapor ranges from 70 to 270 Pa. That is, the partial pressure of water vapor is well below 611.2Pa, which is the corresponding pressure for triple-phase point. Therefore, the frosting characteristics depends on two crucial parameters,  $T_w$  and  $T_f$ .

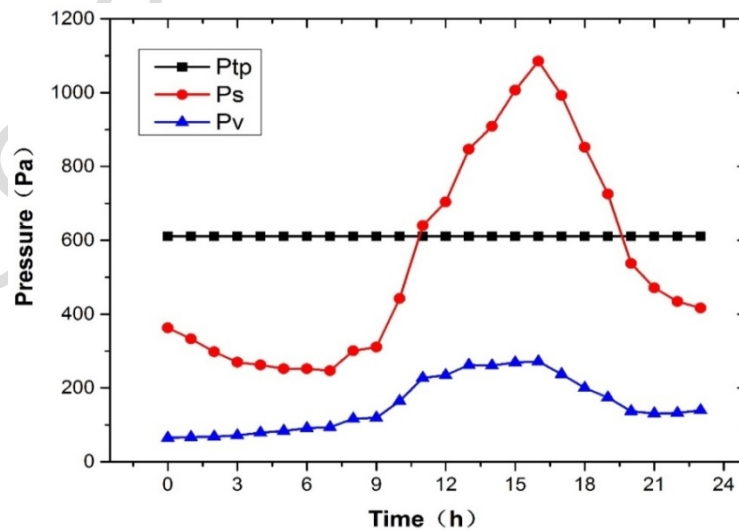


**Fig. 4.** Variation profiles of the partial pressure of water vapor, partial pressure of saturated water vapor and the triple point' corresponding pressure

The sublimation point is determined by the partial pressure of water vapor from the phase diagram of water. The relationship between the partial pressure of water vapor and sublimation point is mapped in Fig.5. The curve evidences an exponential tendency, enabling the use of the exponential regression expressed by:

$$P_v = 619.8 \times e^{0.088T_f} \quad (7)$$

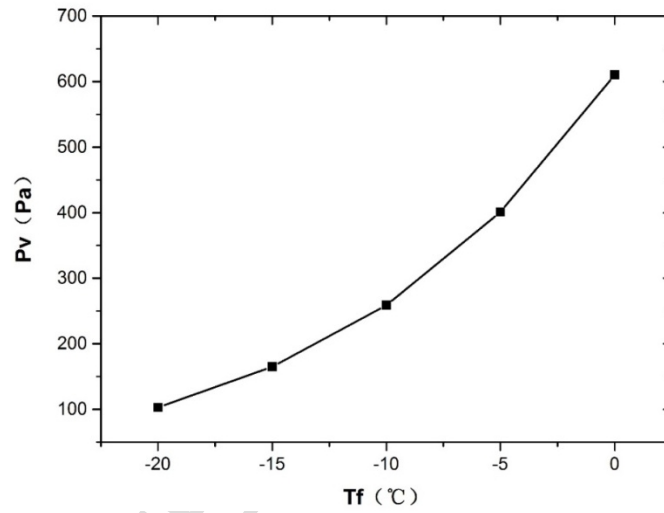


**Fig.5.** The relationship between the partial pressure of water vapor and sublimation point

According to the literature [24], the temperature difference between ambient air and air-side heat exchanger surface is always within a range of 8.12~10.2 °C. The maximum temperature difference of 10.2 °C is used to calculate the air-side heat exchanger surface temperature. The air-side heat exchanger surface temperature can be estimated by using the following correlation:

$$T_w = T_a - 10.2 \quad (8)$$

Fig.6 shows the temperature variation profiles of the heat exchanger surface and sublimation point. The temperature variation tendencies for the heat exchanger surface and sublimation point are similar. The heat exchanger surface temperature is always higher than the sublimation point temperature, and the temperature difference for them is from 1.7 to 9.7 °C, indicating that the ASHP operates under dry condition in winter in Lhasa, the frosting rarely occurs on the evaporator side. A similar conclusion was reported in Rong et al.'s study [25].

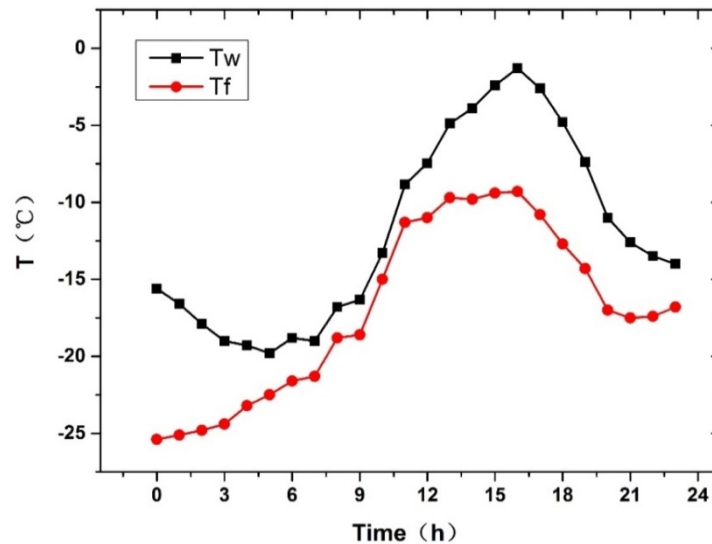


**Fig. 6.** Temperature variations of the sublimation point and heat exchanger surface

### 3. Mathematical modelling of ASHP

A typical ASHP is modeled in this section. The schematic diagram of the ASHP system is shown in Fig. 7(a), where the system mainly consists of a compressor, a condenser, an expansion valve and an evaporator. Fig. 7(b) shows the detailed working process of the ASHP system on pressure-enthalpy diagram. As shown, a 7-



point cycle model is chosen to simulate the entire cycle.

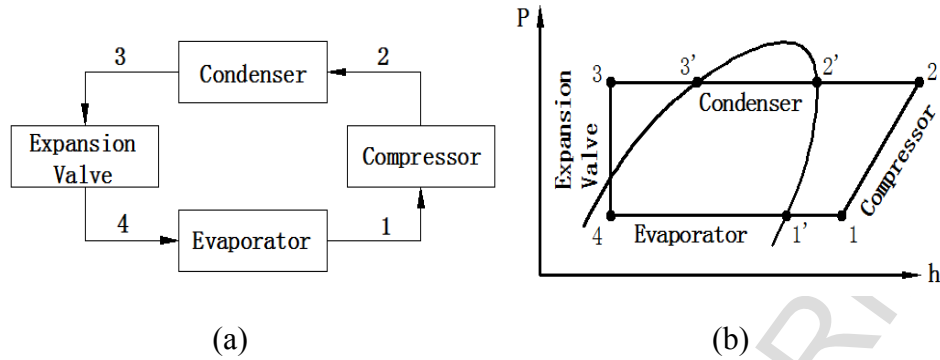


**Fig.7.** (a) Schematic diagram of ASHP (b)  $p-h$  diagram of the cycle

A mathematical model is developed to predict the thermal performance of the ASHP system based on the following assumptions:

- (1) The refrigerant pressure drop in evaporator and condenser is neglected[18,26];
- (2) The isentropic efficiency of the compressor is taken into account;
- (3) The throttling process in expansion valve are isenthalpic;
- (4) The compressing process in compressor is isentropic;
- (5) Average air temperature across the evaporator is considered;
- (6) The system is at quasi-steady state within the chosen time interval.

All the models of the condenser, evaporator, and collector are built by zoned lump parameter method. The models of four components can be combined together according to the relationship between component parameters to calculate the system performance under certain system configuration and operation parameters.

### 3.1. Compressor

The model of the compressor is based on the ideal compression process and makes use of efficiency-based model to predict the compressor performance. The key parameters that are of interest in the compressor model in terms of mass flow rate of refrigerant ( $m_{com}$ ) and electrical input power ( $W_{in}$ ) are expressed as [26]:

$$m_{com} = \frac{nV_d\eta_v}{60v} \quad (9)$$

where  $\eta_v$  is the volumetric efficiency,  $V_d$  is the displacement volume of compressor,  $n$  is the compressor speed.  $v$  is the specific volume of refrigerant gas at compressor suction. The volumetric efficiency,  $\eta_v$  can be given as [27]:

$$\eta_v = 0.959 - 0.006422 \frac{p_c}{p_e} \quad (10)$$

where  $P_c$  and  $P_e$  are the condensing and evaporating pressures, respectively.

The electrical input power of the compressor can be written as:

$$W_{in} = m_r(h_2 - h_1)/\eta_{is} \quad (11)$$

Where  $m_r$  represents the mass flow rate of refrigerant of compressor, and equals to  $m_{com}$ ,  $\eta_{is}$  is the isentropic efficiency, which is given as:

$$\eta_{is} = 0.874 - 0.0135 \frac{p_c}{p_e} \quad (12)$$

### 3.2. Expansion valve

The expansion valve is considered to be isenthalpic. The refrigerant mass flow is calculated as follows [28]:

$$m_{val} = C_{val}(p_b - p_e - \Delta p_{st})(\rho_f \Delta p)^{1/2} \quad (13)$$

where  $C_{val}$  is the characteristic constant of the expansion valve,  $P_b$  is the pressure of thermal bulb,  $\Delta p$  is the pressure difference between the inlet and outlet of the

expansion valve.  $\Delta p_{st}$  is the static pressure provided by the valve's spring.  $C_{val}$  can be calculated according to the nominal work conditions of the valve:

$$C_{val} = \left[ \frac{m_{val}}{(p_b - p_e - \Delta p_{st})(\rho_f \Delta P)^{1/2}} \right]_{nominal} \quad (14)$$

where the subscript nominal represents the nominal work conditions.

$\Delta p$  can be calculated by using the following equation:

$$\Delta p = C_{\Delta p}(p_c - p_e) \quad (15)$$

where  $C_{\Delta p}$  is the coefficient of correction, and an empirical value of 0.55 is used here [27].

For the fully open expansion valve, the Eq. (13) is rewritten as:

$$m_{val} = C_{val, fully}(\rho_f \Delta p)^{1/2} \quad (16)$$

where  $C_{val, fully}$  is the characteristic constant. It is assumed that when the valve is fully open the mass flow rate reaches its maximum value, which is 20% greater than the value of nominal work conditions.  $C_{val, fully}$  is given by:

$$C_{val} = \left[ \frac{1.2m_v}{(\rho_f \Delta p)^{1/2}} \right]_{nominal} \quad (17)$$

The mass flow rate is normally calculated by Eq. (13) while the value is calculated by Eq. (16) refers to the maximal mass flow rate. Therefore, when the value of Eq. (13) is larger than that of Eq. (16), the mass flow rate is equal to the latter one.

### 3.3. Finned-tube evaporator

The atmospheric pressure does not influence the working refrigerant inside the sealed finned tube, so the effect of low-pressure on the heat transfer process of heat

exchanger mainly occurs in the air side. The model of the finned-tube evaporator is developed by zoned lump parameter method. The heat absorption of the finned-tube evaporator ( $Q_{fe}$ ) can be expressed as:

$$Q_{fe} = m_{fe}(h_1 - h_4) \quad (18)$$

where  $m_{fe}$  is the mass flow rate of refrigerant in the finned-tube evaporator.

The total heat absorption of the evaporator  $Q_{fe}$  can also be calculated as:

$$Q_{fe} = \varepsilon_{fe} m_a C_a (T_{a,i} - T_e) \quad (19)$$

where  $\varepsilon_{fe}$  is the heat exchanger effectiveness of the evaporator,  $m_a$  is the mass flow rate of air,  $C_a$  is the air specific heat,  $T_e$  is the evaporating temperature of the refrigerant,  $T_{a,i}$  is the ambient temperature of air

The heat exchanger effectiveness  $\varepsilon_{fe}$  can be calculated as:

$$\varepsilon_{fe} = 1 - \exp(-U_{fe} A_{fe} / m_a C_a) \quad (20)$$

where  $U_{fe}$  is the total heat transfer coefficient of the evaporator.

The total heat transfer coefficient  $U_{fe}$  can be obtained as [29]:

$$U_{fe} = \frac{1}{\frac{1}{h_r A_{fe,o}} + \frac{1}{h_a \eta_f} + r} \quad (21)$$

where  $r$  is the total resistance of the fouling resistance, tube thermal conduction resistance and thermal contact resistance, and an estimated value of 0.0048 is used[30].  $A_{fe,i}$  and  $A_{fe,o}$  are the external and internal areas of the tube, respectively.  $h_r$  and  $h_a$  are the heat transfer coefficients at the refrigerant and the air side, respectively.  $\eta_f$  is the fin efficiency.

### 3.4. Condenser

The model of the condenser is also developed by zoned lump parameter method.

An energy balance of the condenser is expressed as below:

$$m_w C_w (T_{w,o} - T_{w,i}) = m_{con} (h_2 - h_3) = U_c A_c \Delta T_m \quad (22)$$

where  $m_w$  and  $C_w$  are the mass, specific heat of water, respectively.  $T_{w,i}$  and  $T_{w,o}$  are the inlet temperature and outlet temperature of water,  $U_c$  is the total heat transfer coefficient of the condenser,  $A_c$  is the area of the condenser,  $\Delta T_m$  is the log-mean temperature difference.

If the thermal resistance of the condenser tube can be neglected, the total heat transfer coefficient  $U_c$  can be estimated as:

$$U_c = \frac{1}{\frac{A_{c,o}}{A_{c,i} h_{c,r}} + \frac{1}{h_w}} \quad (23)$$

where  $A_{c,o}$  and  $A_{c,i}$  are the external and internal areas of the tube, respectively.

The area of the condenser ( $A_c$ ) can be calculated as:

$$A_c = \alpha_c \cdot L \cdot N \quad (24)$$

where  $\alpha_c$  is the heat exchange area per unit tube length,  $L$  is the length of the tube,  $N$  is the number of the tube.

The log-mean temperature difference  $\Delta t_m$  is obtained as:

$$\Delta t_m = \frac{\Delta t_w - \Delta t_r}{\ln \frac{\Delta t_w}{\Delta t_r}} \quad (25)$$

### 3.5. Heat transfer coefficients

The single-phase heat transfer coefficient ( $h_r$ ) of refrigerant inside the tubes of evaporator is given as follows [29]:

$$Nu = \frac{(f/8)Re \cdot Pr}{1.07 + 12.7\left(\frac{f}{8}\right)^{\frac{1}{2}}(Pr^{\frac{2}{3}} - 1)} = \frac{\lambda_r}{d_i h_r} \quad (26)$$

where  $f$  is the friction coefficient,  $Nu$  is Nusselt Number,  $Re$  is Reynolds Number,  $Pr$  is Prandtl Number,  $\lambda_r$  and  $d_i$  are the thermal conductivity and the inner diameter of the tube, respectively.

The friction coefficient  $f$  is given as :

$$f = (1.82 \ln Re - 1.64)^{-2} \quad (27)$$

The two-phase heat transfer coefficient ( $h_{r,vl}$ ) of refrigerant inside the evaporator can be calculated by the following equation [29]:

$$h_{r,vl} = h_{r,l} \left\{ \left[ (1-x) + 1.2x^{0.4}(1-x)^{0.01\left(\frac{\rho_l}{\rho_v}\right)^{0.37}} \right]^{-2.2} + \left[ \frac{h_{r,v}}{h_{r,l}} x^{0.01\left(1 + 8(1-x)^{0.7\left(\frac{\rho_l}{\rho_v}\right)^{0.67}}\right)} \right]^{-2} \right\}^{-0.5} \quad (28)$$

where  $h_{r,l}$  and  $h_{r,v}$  are the heat transfer coefficients of liquid phase and vapor phase of refrigerant, respectively, and can be obtained by Eq. (26) [29].  $x$  is the quality of refrigerant. For a calculation element of the evaporation or condensation pipes, the specific enthalpy of the inlet refrigerant is already known.  $x$  can be calculated with known specific enthalpy and pressure of refrigerant by using REFPROP [31].  $\rho_l$  and  $\rho_v$  are the densities of the liquid phase and vapor phase, respectively.

The air-side heat transfer coefficient ( $h_a$ ) is given as follows [29]:

$$h_a = \frac{j \rho_a u_{max} C_a}{Pr^{2/3}} \quad (29)$$

where  $j$  is the heat transfer factor and  $u_{max}$  is the wind velocity at the most

narrow interface, and is assumed to be 3 m/s. The heat transfer factor and wind velocity can be estimated by [29]:

$$j = 0.0014 + 0.2618Re^{-0.4\left(\frac{A_{o,f}}{A_o}\right) - 0.15} \quad (30)$$

$$u_{max} = u_w \frac{s_1 s_2}{(s_1 - d_0)(s_f - \delta_f)} \quad (31)$$

where  $A_{o,f}$  and  $A_o$  are the areas of the outer tube with the fin and outer tube, respectively,  $s_1$  and  $s_2$  are the tube spacings along refrigerant flowing direction and vertical direction, respectively,  $d_0$  is the outer diameter of the tube,  $\delta_f$  is the thickness of the fin,  $s_f$  is the fin spacing.

Combining Eq. (30) and (31) into Eq. (29), Eq. (32) is obtained as follows :

$$h_a = \frac{\left(0.0014 + 0.2618Re^{-0.4\left(\frac{A_{o,f}}{A_o}\right) - 0.15}\right)\left(\frac{s_1 s_2}{(s_1 - d_0)(s_f - \delta_f)}\right)\rho_a u_w C_a}{Pr^{2/3}} \quad (32)$$

As stated in Section 2, the air dynamic viscosity  $\mu$ , specific heat  $C_a$  and Prandtl number can be regarded as constant in a certain temperature. However, the air density  $\rho_a$  decreases with the decrease of the atmospheric pressure, the Reynolds number  $Re$  hence decreases with the decrease of the pressure in the case of the constant flow velocity and temperature. Therefore, the atmospheric pressure has a direct effect on the air-side heat transfer coefficient of the evaporator.

The water side heat transfer coefficient ( $h_w$ ) inside the condenser is given by [32]:

$$h_w = 0.5 \frac{\lambda_w}{d_0} \left( \frac{g \beta_w \Delta t d_0^3 \rho_w^2 C_w}{\mu_w \lambda_w} \right)^{0.25} \quad (33)$$

where  $\lambda_w$ ,  $\beta_w$ ,  $\rho_w$  and  $\mu_w$  are the thermal conductivity, thermal expansion

coefficient, density and dynamic viscosity of the water, respectively.

The single-phase heat transfer coefficient ( $h_c$ ) inside the condenser is calculated by the following equation:

$$h_c = 0.023 \frac{\lambda_r}{d_i} Re^{0.8} Pr^{0.3} \quad (34)$$

The two-phase heat transfer coefficient ( $h_{r,vl}$ ) inside the condenser is given by equation:

$$h_{c,vl} = h_{c,l} \left[ (1-x)^{0.8} + \frac{3.8x^{0.76}(1-x)^{0.44}}{Pr^{0.38}} \right] \quad (35)$$

where  $h_{c,l}$  is the liquid-phase heat transfer coefficient, which can be calculated by Eq. (34).

### 3.6. System model

The COP of heat pump is expressed by the following equation:

$$COP = \frac{\text{Heat rejected by the condenser}}{\text{Electrical power input to the compressor}} = \frac{Q_c}{W_{in}} \quad (36)$$

Based on the above-detailed analysis of each component of the ASHP system, a simulation program is written in “MATLAB” software to predict the thermal performance of the ASHP system. The thermodynamic properties of the chosen refrigerant R22 are calculated by using REFPROP software. The models of four components can be combined together according to the relationship between component parameters under certain system configuration and operating parameters. The flowchart of the computer program is shown in Fig. 8.



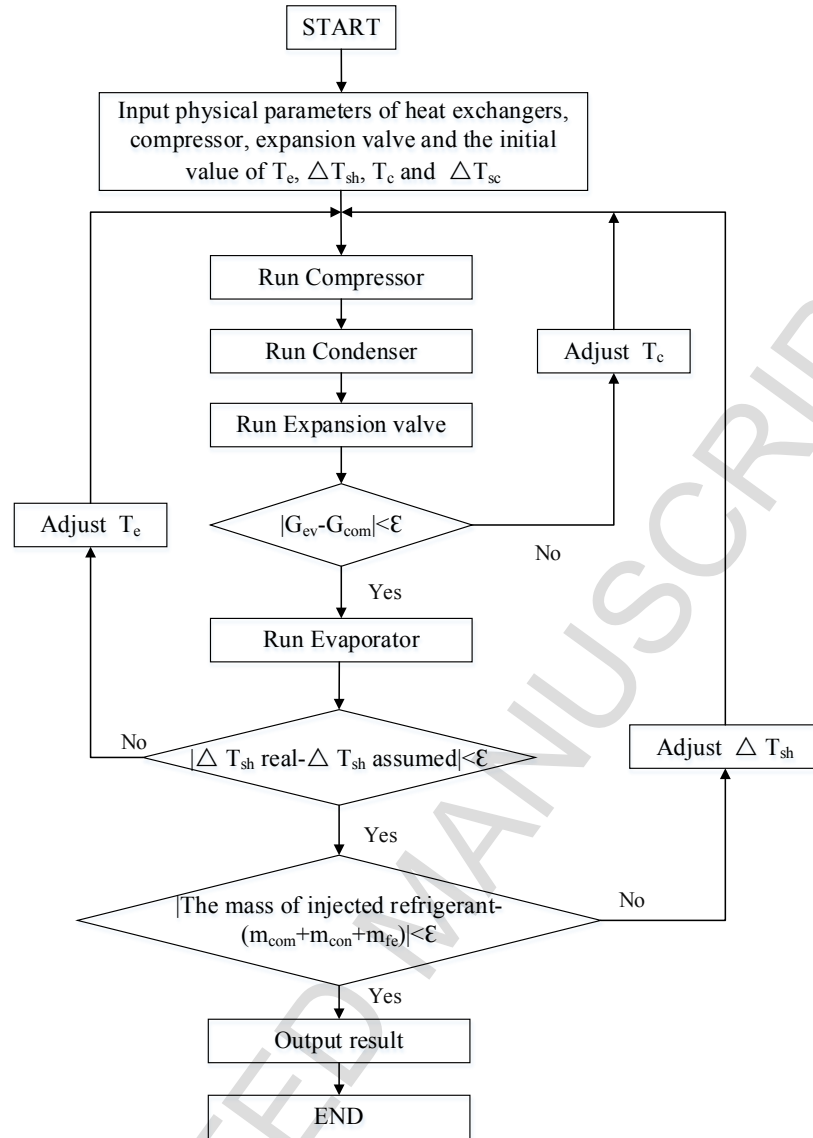


**Fig.8.** Flowchart of the simulation program

#### 4. Validation of the model

In order to study the performance of the ASHPWH system, a series of field experimental work has been carried out in seven ASHPs for an office building in Lhasa during a period of December 24 2014 to December 28 2014 (see Fig.9) . The rated heating capacity and COP of an ASHP unit are 70.0 kW and 3.0, respectively. Table 1 shows more details of the ASHP system. The schematic diagram of the

experimental site is shown in Fig. 10. The heated water (45 °C) from the condenser was pumped into the fan coil and fresh air handling unit and releases heat to air, then the water (40 °C) is circulated back to the evaporator.

During the period of field measurements, outdoor weather conditions varied. Measurements at 16 different outdoor air dry-bulb temperatures were taken. Under each outdoor air dry-bulb temperature, the ASHP system is operated under full load condition.

To determine the actual values of heating capacity and COP at a specific outdoor air temperature, the temperature of inlet and outlet water, the water mass flow rates of the pumps, input power, ambient temperature, relative humidity and wind speed were monitored. The average values of the heating capacity and COP from seven ASHPs are used to compare with the results obtained from the proposed ASHP simulation program.

The meteorological data of Lhasa during the period of testing is given as follows: the ambient air temperature varies from -7.6°C to 15°C, the relative humidity varies within 16.8%~33.4% and the average wind velocity is 3 m/s.

**Table 1**  
Specifications of the main components of the ASHP system

Items	Remarks
Compressor	Speed: 2850 rpm, Displacement volume: 296.8 cm <sup>3</sup> /rev, rated input power: 20.9kW
Condenser	Smooth copper tube: D15*1.2 mm, length of the tube: 950mm, number of the tube:60

Evaporator Front face area:  $0.8968 \text{ m}^2$  , air-side area:  $16.7 \text{ m}^2$ , Thickness of fin: 0.15 mm, Pitch of the fin: 2.3mm, Pitch of the tube in the flowing direction: 19 mm, Pitch of the tube in the vertical direction: 25 mm, smooth copper tube: D 9.52\*0.38 mm

Mass of injected refrigerant 19kg/s



**Fig. 9.** The building equipped with ASHP system in Lhasa, capital of Tibet Autonomous Region of China

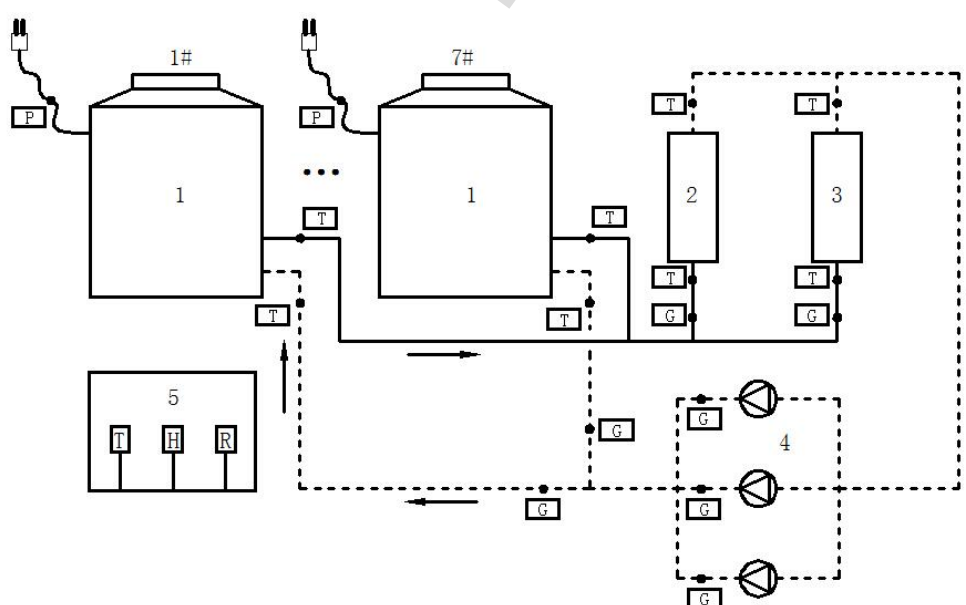


**Fig. 10.** The schematic diagram of the ASHP system for field-testing in Lhasa. 1.

ASHP unit (seven in total), 2. Fan coil, 3. Fresh air handling unit, 4. Water pump, 5.

Air temperature sensors, relative humidity sensors and solar meter

Fig. 11 shows the simulated results of heating capacity and COP versus the corresponding experimental data during a period of 5 days. Fig.12 depicts the average experimental heating capacity and COP versus the results obtained from simulation. For heating operating condition, the experimental heating capacity increases gradually from 43.45 kW to 67.64 kW with the increase of ambient temperature. It is seen that simulated and experimental heating capacities have a similar variation trend. In addition, the figure shows that the simulated results are in good agreement with the experimental data with maximum deviation of 8.2%.

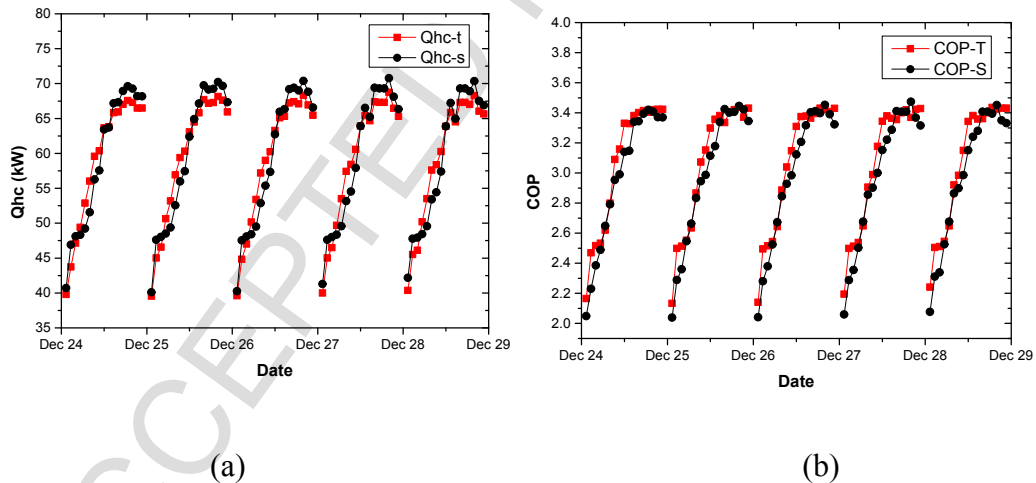
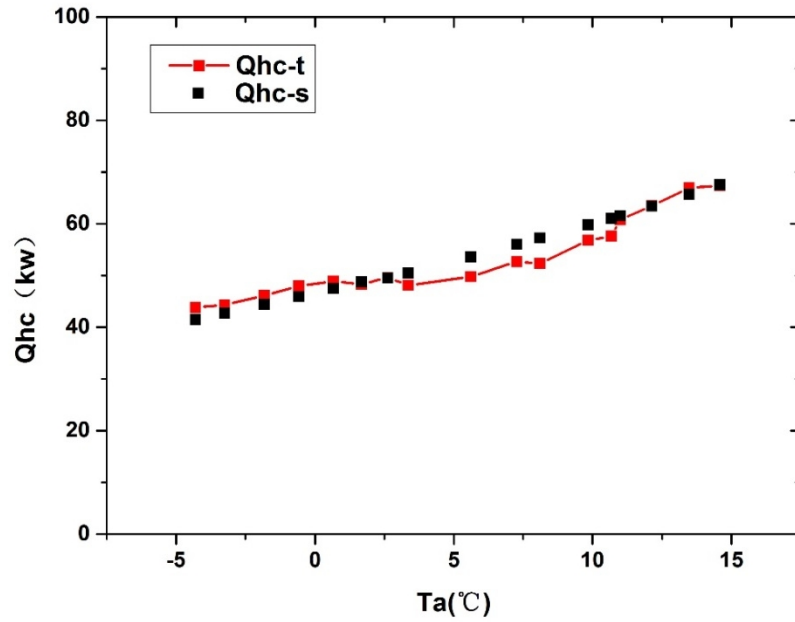


Fig.11. Comparison of simulated data and experimental data from 24 Dec to 28 Dec

2014: (a) heating capacity, and (b) COP



**Fig. 12.** Simulated heating capacity vs. experimental heating capacity

As described above, the heating capacity of the ASHP system in the experiments varies with the ambient temperature, which led to the variation of COP. Fig. 13 shows the simulated and experimental COP variation with the ambient temperature from -5°C to 15°C during heating operation. The COP increases from 2.2 to 3.2 with increasing ambient temperature. The maximum deviation between experimental and simulated results at the same ambient temperature is less than 8 %.

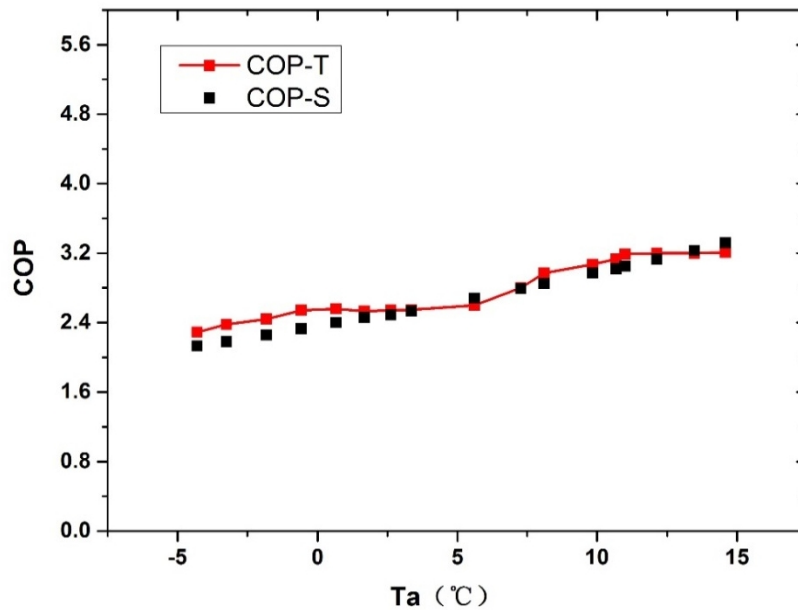


**Fig.13.** Comparison of simulated COP and experimental COP

In addition, whether the frost occurs on the air-side heat exchanger is judged by using observation method during the testing period. The occurrence of frost or condensation on heat exchanger is not found, and the automatic defrost-cycle is not executed as well. It is indicated that the frost hardly occurs during heating operating in winter. This is consistent with the conclusion of the above theoretical analysis.

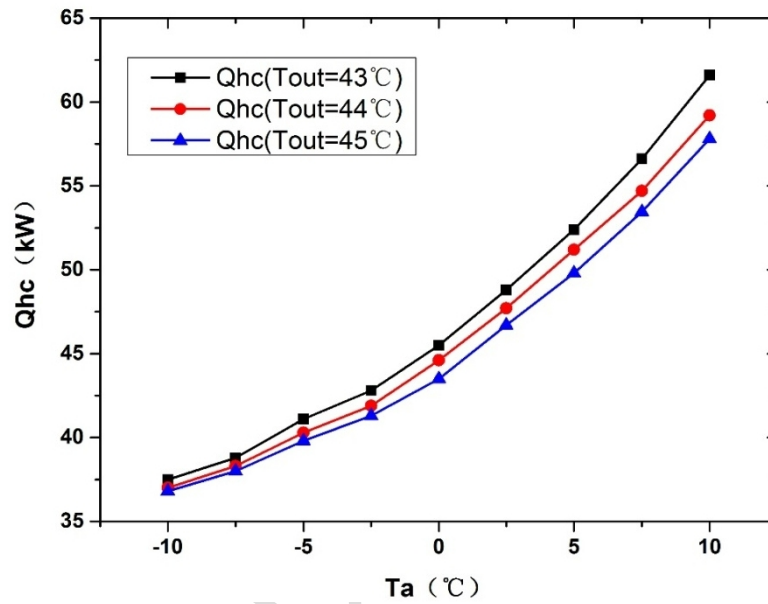
Fig.12 and Fig.13 show a good agreement between the experimental data and the simulated results. Therefore, the numerical model is reliable for further analysis.

## 5. Results and discussion

### 5.1 Effect of the temperatures of the outlet water and ambient air on the performance of the ASHP system

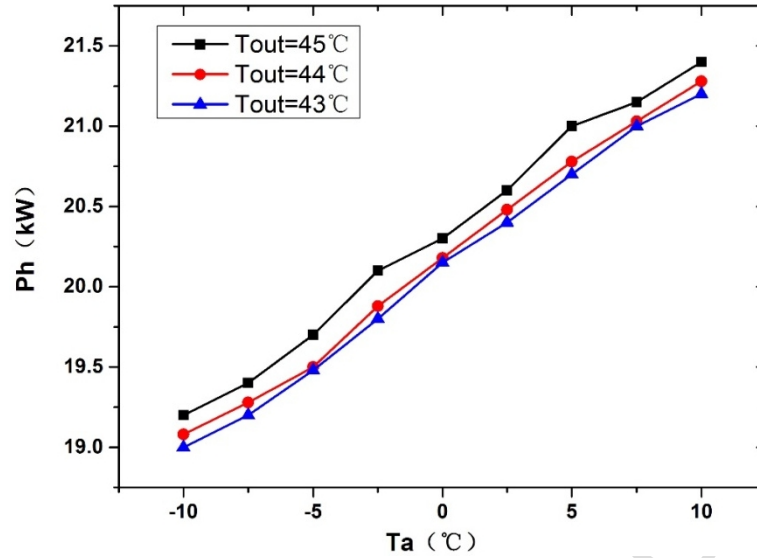
Fig. 14 displays the variations of heating capacity with ambient air temperature for various outlet water temperatures. It is clearly seen that for all studied cases, the

heating capacity is increased with the increase of ambient air temperature. The heating capacity can be increased by 45% for outlet water temperature of 45 °C when ambient temperature is increased from -10.0 °C to 10.0 °C. However, the heating capacity decreases with the increase of water temperature, and the heating capacity difference is increased with the ambient temperature increasing.



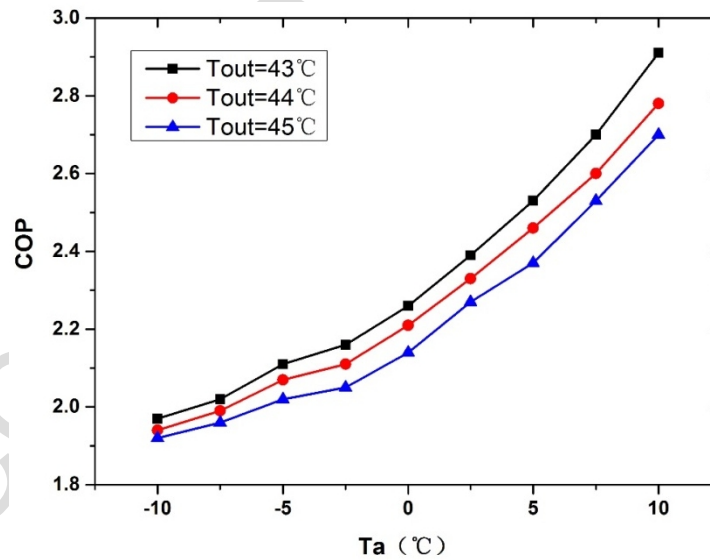
**Fig.14.** Heating capacity vs. ambient air temperature for various outlet water temperatures

Fig. 15 illuminates the variations of input power with outlet water temperature for various ambient air temperatures. As shown, the input power of the ASHP system increases with the increase of ambient temperature and water temperature. The input power increases from 19.2 kW to 21.4 kW for outlet water temperature of 45 °C when ambient temperature increases from -10.0 °C to 10.0 °C.



**Fig.15.** Input power vs. ambient air temperature for various outlet water temperatures

Fig. 16 displays the variations of COP with the ambient air temperature for various water temperatures. Similar to the heating capacity, the COP increases with the increase in the ambient air temperature or with the decrease in water temperature.



**Fig.16.** System COP vs. ambient air temperature for various outlet water temperatures

## 5.2. Effect of the atmospheric pressure on the system performance in high



**altitude area**

As stated previously, the atmospheric pressure has a direct impact on the system performance of the ASHP system. In order to assist the engineers in selecting suitable ASHP system for a specific project in high altitude area, it is essential to study its effect on the system performance by comparing the system performance in high altitude area and plain area. In this part, all input parameters of the system and meteorological data are same for the system models for high altitude area and plain area except the factor of altitude, which is assumed that 0 m for plain area and 3680 m for Lhasa.

Fig.17 displays the variations of heating capacity with ambient air temperature for Lhasa and plain area. As shown, the heating capacity of the ASHP system in Lhasa is much lower than that for plain area. The heating capacity of the system in Lhasa is increased from 33.70 to 60.86 kW with the ambient temperature increases from -12 to 10 °C, while the heating capacity of the system in plain area is increased from 40.18 to 75.86 kW. The ratio of the heating capacity in Lhasa to that for plain area varies within 80.2 % to 83.8 %. This is due to the heat transfer coefficient of airside decreases with the decrease of the atmospheric pressure, which has decreased by 15% in Lhasa when compared to standard pressure (101.325 kPa). This is due to that the heat transfer coefficient affects the heating capacity in a complicated process. When the heat transfer coefficient reduces, the heat transfer in both evaporator and condenser, the temperature difference of evaporator and condenser and the refrigerant

536 flow rate are changed as well. The combined effect reduces the heating capacity  
537 observably.

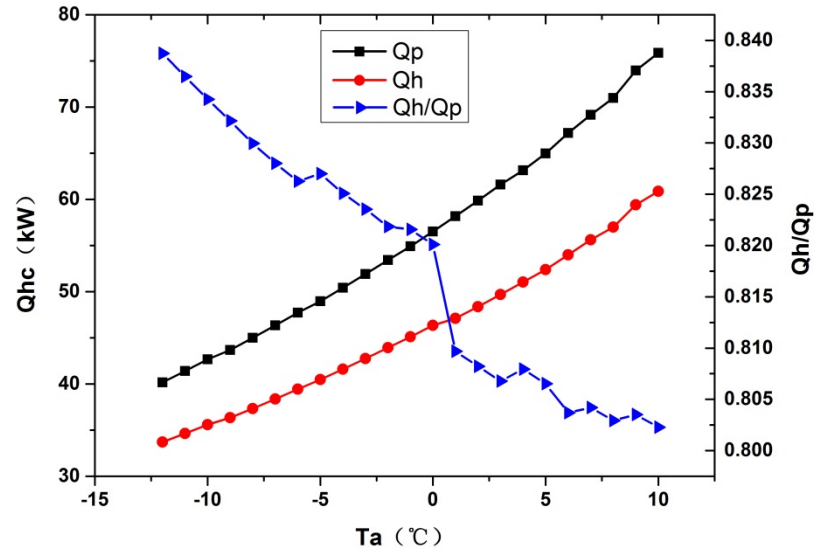


**Fig.17.** Comparison of the heating capacity of system in Lhasa and plain area

541 Fig.18 shows the variations of COP with ambient air temperature for Lhasa and  
542 plain area. It is seen that the COP of the ASHP system in Lhasa is lower than that for  
543 plain area. The COP of the system in Lhasa is increased from 1.76 to 2.87 with the  
544 ambient temperature increases from -12 to 10  $^{\circ}\text{C}$ , while the COP of the system in  
545 plain area is increased from 1.94 to 3.27. The ratio of the COP in Lhasa to that for  
546 plain area varies within 87.5 % to 90.5 %, and the ratio of COP is higher than that for  
547 heating capacity. This is due to the input power of the compressor is changed little  
548 while the input power of the fan is decreased. According to the definition of the power  
549 similarity law of fan, the input power of the fan is linear proportional to the air density

[33], which is reduced 35 % in Lhasa when compared to standard pressure (101.325 kPa).

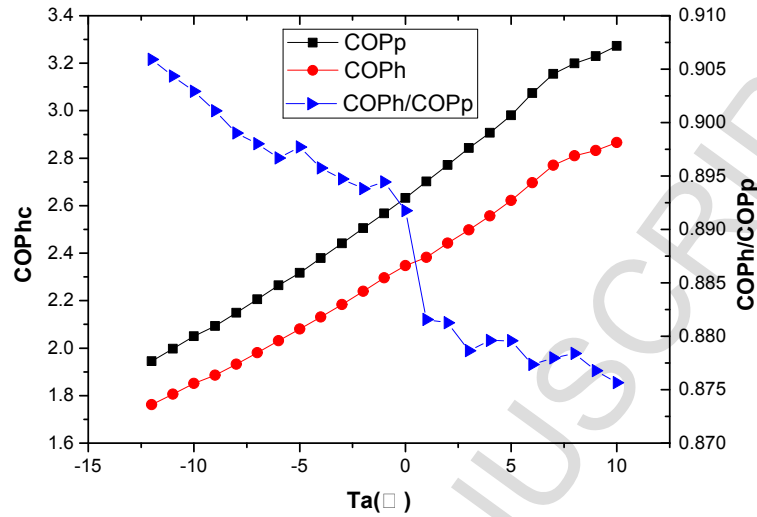


**Fig.18.** Comparison of the COP of system in Lhasa and plain area

From the simulation results above, it is known that the thermal performance of the ASHP system is greatly influenced by the altitude and ambient air temperature. Therefore, it is important to consider the two factors in selection of the ASHP system in high altitude area. According to literature [34], the outdoor design temperature for winter air conditioning for Lhasa is  $-8^{\circ}\text{C}$ , the correction coefficient of the rated heating capacity of the ASHP system is 0.83 based on the results of Fig.17.

### 5.3. Comparison of the heating capacity of ASHP in Lhasa and other cities

The heating capacity of the ASHP system in Lhasa is compared with that for other cities by considering the evaporator-frosting problem. The reference [35] gave the frost loss coefficient of some cities in China, such as Wuhan, Shanghai, Chengdu,

can reach 0.87–0.94, and Jinan, Xi'an can be high up to 0.75 (see Table 2).

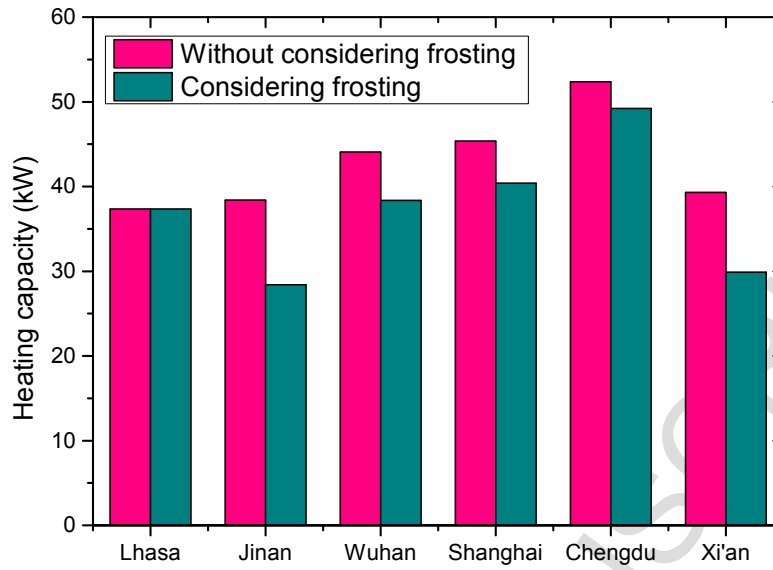
**Table 2**

The frost loss coefficient of the ASHP system in some cities of China

City	Relative humidity of coldest month (%)	Outdoor design temperature for winter air conditioning (°C)	Loss coefficient
Jinan	54	-10	0.74
Xi'an	67	-9	0.76
Wuhan	76	-5	0.87
Shanghai	75	-4	0.89
Chengdu	80	1	0.94

Fig.19 illustrates the heating capacity of the ASHP system for Lhasa and other cities in China for the cases of without considering frosting problem and considering frosting problem. In the case of without considering frosting problem, the heating capacities of the system for studied cities are 52.2 kW (Chengdu), 45.4 kW (Shanghai), 44.1 kW (Wuhan), 39.3 kW (Xi'an), 38.4 kW (Jinan), and in Lhasa is 37.5 kW, respectively. It is seen that the heating capacity of ASHP in Lhasa is lowest amongst six cities. However, for the case of considering frosting problem, the actual heating capacity of the system in Lhasa is 37.5 kW, which is greater than that for Jinan (28.4 kW) and Xi'an (30 kW), and is nearly same to Wuhan (38.1 kW), while is lower than that for Chengdu (49.3 kW). This shows that the frosting on evaporator can greatly reduce the performance of ASHP. The heating capacity of system in Lhasa

581 is almost same or higher than most cities when considering frosting problem.



582

583 **Fig.19.** Comparison of heating capacity of ASHP in Lhasa and other cities in China in  
 584 cases of without considering frosting problem and considering frosting problem

585

586 Fig.20 depicts the actual COP of the ASHP system for Lhasa and other cities in China  
 587 when considering frosting problem. It is seen that the actual COP of the system in  
 588 Lhasa is 1.98. Similarly, the system's COP in Lhasa is higher than that for Jinan  
 589 (1.57) and Xi'an (1.61), and is close to that for Wuhan (2.01), while is lower than that  
 590 for Chengdu (2.36). In sum, though the atmospheric pressure in Lhasa is lower than  
 591 other cities, the low relative humidity prevents the evaporator from frosting problem.  
 592 The ASHP system possesses convincing potential of practical application in high  
 593 altitude area.

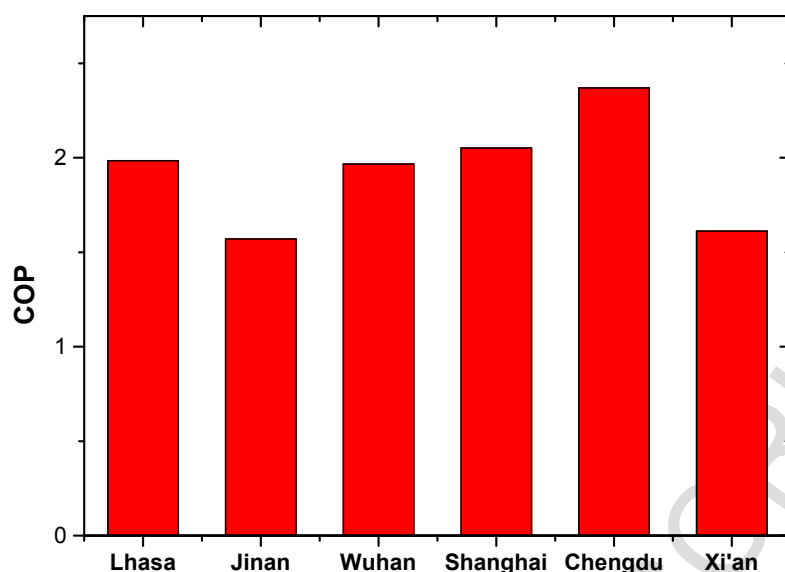


**Fig.20.** Comparison of COP of ASHP in Lhasa and other cities in China

## 6. Conclusions

In this study, an experimentally validated numerical model is developed to investigate the performance of an ASHP system in Tibetan weather conditions. The research shows that the ASHP system presents convincing potential of practical application in high altitude area. The major findings are summarized as follows:

- (1) Theoretical analysis shows that the air side heat exchanger of evaporator is not easy to frost due to the low relative humidity in Lhasa. The theoretical conclusion is consistent with the observed findings for a period of 5 days. Certainly, in order further to verify these results, a complete heating season observation of the frosting characteristics of the ASHP is still required in the next step.
- (2) The numerical results show that the ambient air temperature and atmospheric pressure have a great effect on the system performance. However, the outlet water

temperature has less impact on the performance of the ASHP system.

(3) The study indicates that the low air pressure has a great impact on the performance of ASHP. For the case of considering frosting problem, the COP of the system is increased from 1.76 to 2.87 with ambient temperature increases from -12 to 10 °C, which is reduced by 9.5 % - 12.5 % than that for standard pressure (sea level). The heating capacity of the system increases from 33.70 to 60.86 kW, which is reduced by 16.2 % to 19.8 % than that for standard pressure. For the case of considering frosting problem, the heating capacity and COP of the ASHP system in Lhasa are 37.5 kW and 1.98, respectively under the outdoor design temperature, which are almost same or higher than most cities in this study.

## Acknowledgement

The work described in this manuscript was supported by National Science Foundation of China (No. 51478058), the 111 Project (No. B13041) and Sichuan Science and Technology Support Program (No. 2014GZ0133). The authors are thankful to anonymous reviewers for their valuable comments and feedback.

## References

- [1] Wang Q, Qiu H. Situation and outlook of solar energy utilization in Tibet, China. *Renew Sustain Energy Rev* 2009; 13: 2181–2186.
- [2] Luo G, Zhang X. Universalization of access to modern energy services in Tibetan rural households—Renewable energy's exploitation, utilization, and policy

- analysis. *Renew Sustain Energy Rev* 2012; 16: 2373–2380.
- [3] Ma H, Oxley L, Gibson J. China's energy situation in the new millennium. *Renew Sustain Energy Rev* 2009; 13(8):1781–99.
- [4] Liu G, Lucas M, Shen L. Rural household energy consumption and its impacts on eco-environment in Tibet: taking Taktse county as an example. *Renew Sustain Energy Rev* 2008; 12(7):1890–908.
- [5] Jiang JG, Lou ZY, Ng SL, Luobu CR, Ji D. The current municipal solid waste management situation in Tibet. *Waste Manage* 2009; 29(3):1186–91.
- [6] Gao X, Yu Q, Gu Q, Chen Y, Ding K, Zhu J, et al. Indoor air pollution from solid biomass fuels combustion in rural agricultural area of Tibet, China. *Indoor Air* 2009; 19(3):198–205.
- [7] Song S. Coal resources characteristic. Supply and demand situation analysis in Qinghai Province. *Resour Ind* 2006; 8(2):23–25.
- [8] Junfeng L, Runqing H, Yanqin S, Jingli S, Bhattacharya SC, Abdul Salam P. Assessment of sustainable energy potential of non-plantation biomass resources in China. *Biomass and Bioenergy* 2005; 29(3):167–77.
- [9] Wei X, Yang P, Wang Y, Xie Z. Use of rural energy resources and eco-environmental degradation in Tibet. *J Environ Sci-China* 2004; 16(6):1046–1050.
- [10] Wu W, You T, Wang B, Shi W, Li X. Evaluation of ground source absorption heat pumps combined with borehole free cooling. *Energy Convers Manage* 2014; 79: 334–343.
- [11] Wu W, Zhang X, Li X, Shi W, Wang B. Comparisons of different working pairs and cycles on the performance of absorption heat pump for heating and domestic hot water in cold regions. *Appl Therm Eng* 2012; 48: 349–358.
- [12] Genon G, Torchio MF, Poggio A, Poggio M. Energy and environmental assessment of small district heating systems: global and local effects in two case studies. *Energy Convers Manage* 2009; 50 (3): 522–529.
- [13] Wang W, Feng YC, Zhu JH, Li LT, Guo QC, Lu WP. Performances of air source heat pump system for a kind of mal-defrost phenomenon appearing in moderate climate conditions. *Appl Energy* 2013; 112:1138–1145.
- [14] Kwon O, Cha D, Park C. Performance evaluation of a two-stage compression heat pump system for district heating using waste energy. *Energy* 2013; 57:375 - 81.
- [15] Ibrahim O, Fardoun F, Younes R, Louahlia-Gualous H. Air source heat pump water heater: Dynamic modeling, optimal energy management and mini-tubes condensers. *Energy* 2014; 64: 1102-1116.
- [16] Kamel RS, Fung AS. Modeling, simulation and feasibility analysis of residential BIPV/T + ASHP system in cold climate—Canada. *Energy Build* 2014; 82: 758–770.
- [17] Ugursal VI, Ma B, Li C. Thermal performance and economic feasibility of a low energy house equipped with an air-source heat pump. *Am Soc Mech Eng* 1992;



- 28: 111–117.
- [18] Wu W, Wang B, Shi W, Li X. Techno-economic analysis of air source absorption heat pump: Improving economy from a design perspective. *Energy Build* 2014; 81: 200–210.
- [19] Zhu Y, Yao L, Li X. Calculation method of atmospheric density on fixed geometry height. *Meteorological* 2002; 2:9-12.
- [20] Li Y, Li YC, Liu J. Calculating heat transfer of radiators for plateau vehicles. *J. Huazhong Univ. of Sci. & Tech. (Natural Science Edition)* 2009; 37(9): 90-93.
- [21] Chen Z. Lecture on heat transfer. Beijing: Higher Education Press. 1989.
- [22] Wan J. Theory and properties of fluid molecules. Harbin: Harbin Engineering University press, 1994.
- [23] China Meteorological Administration, Tsinghua University, Weather Data for Built Environment Thermal analysis of China, Beijing: China Archi. Buil. Press. 2005.
- [24] Yan Q, Shi W, Tian C. Refrigeration technology for air conditioning. Beijing: China Archi. Buil. Press. 2010.
- [25] Rong X, Min X, Si P, Gao Q. Suitability analysis for Lhasa heating techniques. *Heating Ventilating Air Conditioning* 2013; 43(6):23-30 (in Chinese).
- [26] X.Q. Kong, D. Zhang, Y. Li, Q.M. Yang. Thermal performance analysis of a direct-expansion solar-assisted heat pump water heater. *Energy* 2011; 36: 6830-6838.
- [27] Brunin O, Feidt M, Hivet B. Comparison of the working domains of some compression heat pumps and a compression-absorption heat pump. *Int J Refrig* 1997; 20:308–18.
- [28] Fu L, Ding G, Zhang C. Dynamic simulation of air-to-water dual-mode heat pump with screw compressor. *Appl Therm Eng* 2003; 23: 1629–1645.
- [29] Deng W, Yu J. Simulation analysis on dynamic performance of a combined solar/air dual source heat pump water heater. *Energy Convers Manage* 2016; 120: 378–387.
- [30] Wu YZ. Principles of refrigeration and cryogenic. Beijing Higher Education Press; 2004.
- [31] Lemmon EW, Huber ML, McLinden MO. NIST thermodynamic and transport properties of refrigerants and refrigerant mixtures (REFPROP) version 8.0. NIST; 2007.
- [32] Kuang YH, Sumathy K, Wang RZ. Study on a direct-expansion solar-assisted heat pump water heating system. *Int J Energy* 2003; 27:531–48.
- [33] Fu X. Fluid transmission and distribution network. Beijing: China Archi. Buil. Press. 2006 (in Chinese).
- [34] China Academy of Building Research. Design code for heating ventilation and air conditioning of civil buildings. Beijing: China Archi. Buil. Press. 2012 (in Chinese).

- 
- [35]Ren J, Jiang J. Characteristics of air source heat pump units. In: Proceedings of  
the 2001 national heat pump and air conditioning technology. Ningbo, China;  
2001 (in Chinese).

**Highlights**

1. The atmospheric has a direct impact on the physical properties of air.
2. The air-side heat exchanger is not easy to frost in Lhasa's weather conditions.
3. Ambient temperature and air pressure have a big impact on the system performance.
4. ASHP shows convincing potential of practical application in high altitude area.